Experimental investigation and kinetic-theory-based model of a rapid granular shear flow

R. D. WILDMAN[1], T. W. MARTIN[1], J. M. HUNTLEY[1], J. T. JENKINS[2], H. VISWANATHAN[1], X. FEN[3] AND D. J. PARKER[3]

[1]School of Mechanical and Manufacturing Engineering, Loughborough University,
Loughborough LE11 3TU, UK
[2]Department of Theoretical and Applied Mechanics, Cornell University, Ithaca, NY 14853 USA
[3]School of Physics and Astronomy, University of Birmingham, Edgbaston, Birmingham B15 2TT, UK

An experimental investigation of an idealized rapidly sheared granular flow was performed to test the predictions of a model based on the kinetic theory of dry granular media. Glass ballotini beads were placed in an annular shear cell and the lower boundary rotated to induce a shearing motion in the bed. A single particle was tracked using the positron emission particle tracking (PEPT) technique, a method that determines the location of a particle through the triangulation of gamma photons emitted by a radioactive tracer particle. The packing fraction and velocity fields within the three-dimensional flow were measured and compared to the predictions of a model developed using the conservation and balance equations applicable to dissipative systems, and solved incorporating constitutive relations derived from kinetic theory. The comparison showed that kinetic theory is able to capture the general features of a rapid shear flow reasonably well over a wide range of shear rates and confining pressures.

1. Introduction

Granular materials are employed in a variety of guises in industrial processes to aid the transport and storage of a range of products. These materials can be induced to flow through, for example, vibration (Clement & Rajchenbach 1991), shearing (Hsiau & Shieh 1999) and gas flow (Tsuji, Morikawa & Shiomi 1984) and under these conditions their behaviour resembles that of a fluid or a gas. This qualitative similarity can be placed on a firmer mathematical footing through the use of, for example, the kinetic theory developed originally for the description of thermal fluids (Chapman & Cowling 1970). Over the last 30 years this approach has gained in popularity and evolved in sophistication as researchers have aimed for a description of granular flow through the use of a continuum or hydrodynamic equation set (Jenkins & Savage 1983; Jenkins & Richman 1985*b*; Jenkins & Mancini 1989; Johnson, Nott & Jackson 1990; Zamankhan 1995; Kumaran 1998*a*; Lu, Gidaspow & Manger 2001). Though certain constraints are usually required (low inelasticity, small gradients and so forth; recent work has suggested that a kinetic theory can be derived for all inelasticities (Garzo & Dufty 1999)), this method has shown great promise in

describing granular flows and in a sense is successful in describing flows where strictly speaking these assumptions cannot be guaranteed to hold.

Various geometries have been used as test systems for granular theories. In particular, vibrated systems have proved a useful tool for investigating the effectiveness of granular theories. Commonly a piston drives either a boundary or the complete system. The behaviour of the bed can, under some conditions, be correlated with the motion of the base (Umbanhowar, Melo & Swinney 1996; Bizon *et al.* 1998). When the frequency of the vibration is much larger than the frequency of a bead meeting the base, however, then one can reasonably assume that the bed is decorrelated from the base motion and the energy input can be characterized by the peak base velocity or amplitude of vibration (Luding, Herrmann & Blumen 1994; Warr, Huntley & Jacques 1995). The energy in the bed is then distributed through the collisional interactions between the particles in the container, and the energy input at the base is balanced by the dissipation during collisions between grains and between the grains and the sidewall (Warr *et al.* 1995; Kumaran 1998b; McNamara & Luding 1998, Sunthar & Kumaran 1999; Wildman *et al.* 2000; Wildman, Huntley & Parker 2001b). In simulation and experiment it has been observed that convection currents are small (Wildman, Huntley & Parker 2001a; Talbot & Viot 2002), allowing the momentum conservation to be expressed in the form of the barometric equation and allowing the non-isotropic part of the stress tensor to be neglected (Helal, Biben & Hansen 1997; Wildman *et al.* 2001b). This last step simplifies the equations rather neatly, but in this situation one cannot address the question of the appropriate form of the stress tensor, a key question in understanding granular flows (Volfson, Tsimring & Aranson 2003).

Recently, Martin, Huntley & Wildman (2005) developed a radially averaged model that predicts both the granular temperature variation and the packing fraction as a function of altitude. This included the effect of the dissipation at the walls in an averaged way, but did not lead to prediction of any radial variation. Subsequently, Viswanathan *et al.* (2006) have taken a similar approach and solved the equations with the variables retained as two-dimensional quantities, allowing the granular temperature and packing fraction to be predicted as a function of both height and radius. In both cases, two forms of the heat transfer constitutive law were used. First, following Jenkins & Richman (1985a), the heat flux was derived to be proportional to the temperature gradient, with the coefficient given by the thermal conductivity coefficient. Secondly, the heat flux was derived to be a function of the concentration or packing fraction gradient (Brey *et al.* 1998; Sela & Goldhirsch 1998). The most notable result of modifying the heat law to include a concentration gradient term is a prediction that the granular temperature does not decay to an asymptotic value; rather it increases, somewhat counter-intuitively, with increasing altitude (Brey *et al.* 2001; Martin *et al.* 2005). This last feature is the subject of some debate, and to date has not been resolved satisfactorily. This model has also been tested in experiments performed using magnetic resonance imaging (MRI) (Yang *et al.* 2002; Huan *et al.* 2004) indicating a significant rise in granular temperature in both the vertical and horizontal directions, a feature not reproduced elsewhere (Warr *et al.* 1995; McNamara & Luding 1998; Wildman *et al.* 2001b).

A more robust test of kinetic theories of granular flows can be performed where there is significant shear. Here, one encounters a more complex stress distribution in the system and the possibility of a slip velocity at the boundary (Jenkins & Askari 1999). Simple shear geometries have long been considered as potential systems for a granular 'rheometer'; however, the presence of shear bands, stress chains and lasting contacts, not apparent in fluids, has created considerable barriers to building up
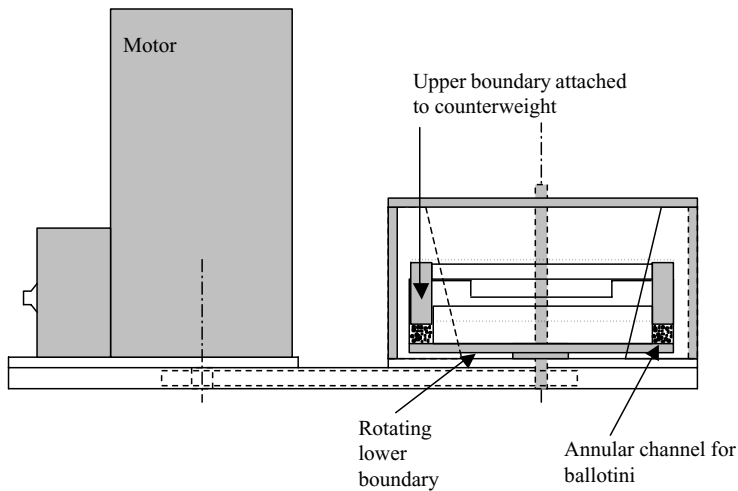
FIGURE 1. A side-view schematic showing the design and layout of the annular shear cell. The particles are confined to a small channel, 25 mm wide, by two PMMA sidewalls. The particles are driven from below by a toothed aluminium boundary and topped by another aluminium toothed surface. The upper surface is able to move in the vertical direction, but is fixed in the azimuthal direction.

a framework of understanding even in apparently simple systems (Campbell 2002; Louge 2003; Volfson *et al.* 2003; MIDI 2004). A notable antecedent of our work is the paper by Savage & Sayed (1984) who constructed a pressure-controlled annular shear cell and measured the relationship between the shear force and the apparent shear rate, and found broad agreement between their results and their proposed stress constitutive law. However, they were unable to view the internal structure of the material or the motion of the individual grains in the bulk. Consequently, they were only able to compare their results with volume-averaged quantities and were not able to test the validity of their model in detail.

In this paper we present the first steps towards being able to probe experimentally the internal behaviour of sheared granular flows. We describe measurements of velocity fields and packing fraction using a non-invasive method of measuring granular flow behaviour. We show, for the first time, the behaviour of model grains inside a three-dimensional annular shear cell and compare these results with a model derived from kinetic theory. We present first the geometry and the positron emission particle tracking (PEPT) system for measuring the particle motion. In § 3 we give distributions of granular behaviour, and also show how the axially varying distributions scale with the base speed and pressure. In § 4 we present a one-dimensional model of a shear flow based on the kinetic theory of granular gases, and in § 5 compare model predictions with experimental results.

2. Experiments details

2.1. *Experimental geometry and PEPT*

We examine the behaviour of a granular flow in a three-dimensional annular shear cell. As can be seen in figure 1, this is a recirculating device similar in design to that developed by Savage & Sayed (1984). There are some differences, however. Our shear cell is driven from below, whilst the top boundary is kept static in the azimuthal

1.67 mm ↓   5.10 mm

FIGURE 2. Profile of the upper and lower boundaries. The pitch at the inner wall is 4.9 mm, and at the outer wall is 5.3 mm. The depth of the teeth is 1.42 mm at the inner wall and 1.92 mm at the outside. The figure shows the average pitch and depth of the teeth.

Position-sensitive
γ-ray detectors

z
x
y

Shear cell

Back-to-back 511 keV photons from
positron emission particle tracking
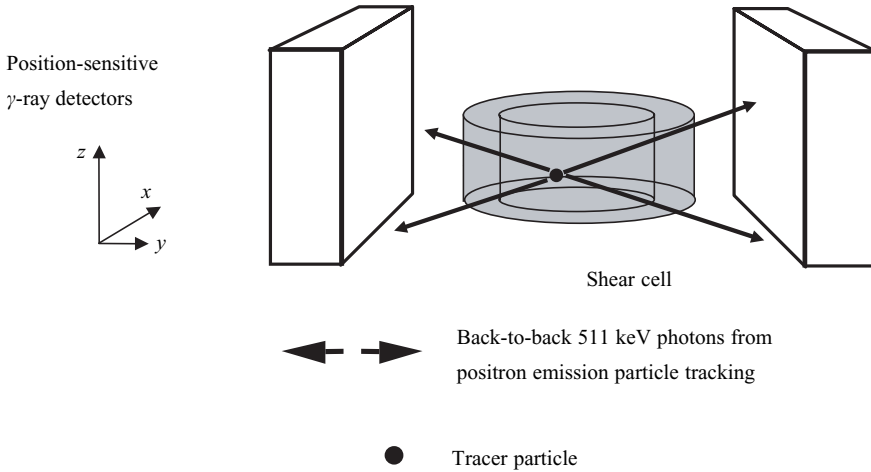
● Tracer particle

FIGURE 3. Position of the annular shear cell in relation to the gamma ray detectors used in the positron emission particle tracking (PEPT) facility.

direction, but is free to move in the vertical direction to allow it to respond to the pressure exerted on it by the particles impacting on it from below. In this configuration we do not measure the torque exerted on the boundary. The sidewalls are made from polymethylmethacrylate (PMMA) with the inner and outer walls of the cell situated respectively 120 mm and 125 mm from the axis. The driving, basal, boundary is interchangeable, and in this paper we use a sawtooth profile base, constructed from aluminium (figure 2). The depth of the teeth at the inner wall is on average 1.42 mm whilst the depth at the outer wall is 1.92 mm, with a linear variation between, and there are approximately 22.8 teeth rad^{-1}. The top and bottom boundaries are identical to one another. The pressure pushing down on the top boundary was varied using a counterweight, creating a pressure-controlled cell. The beads used were ballotini beads of average diameter, $\sigma = 3$ mm, and average mass $m = 3.9 \times 10^{-5}$ kg. One layer of the grains was used in the experiments, where one loose-packed layer of particles consisted of $N \sim 1740$ ballotini beads. The coefficients of restitution for particles against a flat plate, measured using high-speed photography, were particle–particle, $e = 0.91$, particle–sidewall, $e_w = 0.80$ and particle–base, $e_b = 0.79$.

A single particle in the flow was tracked using positron emission particle tracking (PEPT) (figure 3). PEPT works through the detection of 511 keV γ-photons that result from the annihilation event that occurs when a positron encounters an electron. The tracer particles are formed through the irradiation of a ballotini bead with ^{3}He particles resulting in the formation of ^{18}F, leaving the macroscopic properties of the particle unaffected and so the tracer particle is then identical to the remaining beads. ^{18}F is an unstable radioisotope of fluorine and decays through the emission of positrons. A collision between a positron and an electron occurs rapidly and

results in two γ-photons moving on the same path but in opposite directions. These are detected simultaneously, without collimation, by NaI scintillator-based photon detectors. The tracer particle coordinates are then determined through triangulation of successive photon detections, allowing the coordinates to be detected at a rate up to about 1 kHz, at an accuracy of up to $+/-$ 1 mm (Parker *et al.* 1997; Wildman & Parker 2002).

The experiments were performed as follows. The particles, including the tracer particle, were placed inside the shear cell and the top boundary loaded. The shear cell was moved into the field of view of the photon detectors with one edge of the annular channel wholly within the field of view. This ensured that as the tracer particle navigated its way round the shear cell, there would be at least one point in its circuit where it would pass through the most sensitive region of the field of view. Of course, this has a drawback; when the tracer was on the opposite side of the shear cell, the accuracy was correspondingly lower. Once the shear cell had reached the desired speed, the motion of the tracer particle was followed for 30 minutes. Subsequently, the coordinates of the tracer particle were output into a time-stamped list for analysis.

2.2. *Data analysis*

Prior to calculating the fields of interest, the experimental volume was partitioned into small volume elements as a function of height along the axis direction, z, radial distance from the axis, r, and azimuthal direction, θ. This approach enabled the hydrodynamic fields of interest, e.g. the packing fraction, η, and velocity field, v, to be determined as a coarse-grained function of position. Unfortunately, as will be discussed below, though granular temperature is an important hydrodynamic field, it was not possible to measure this in the current set-up.

2.2.1. *Packing fraction*

When only following the motion of a single particle, it is not possible to make a direct measurement of the packing fraction. In a closed, ergodic system, however, it is possible to deduce the average concentration of particles in a volume element by considering the fraction of time spent in the volume element by the tracer particle over the course of the experiment. We make the assumption that the system is ergodic (Wildman *et al.* 2000). In this case the packing fraction is related to the fraction of time the tracer particle resides in a region by

$$\eta_i = \frac{F_i N \pi \sigma^3}{6 V_i} \tag{1}$$

where F_i is the fraction of time the tracer particle has spent in volume element i, V_i is the volume of the element, σ is the particle diameter and N is the total number of particles in the system (Wildman *et al.* 2000).

2.2.2. *Granular temperature*

The granular temperature, T, is defined as

$$T = \tfrac{1}{3} m \overline{C^2} \tag{2}$$

where C is the speed of a particle relative to the mean velocity and m is the particle mass. The granular temperature is in effect a measure of the energy of the fluctuations of the velocities of the grains about the mean velocity. In addition, we may define the

granular temperatures of the grains in different directions, T_z, T_r and T_θ, such that

$$T_j = m\overline{(v_j - \overline{v_j})^2} \tag{3}$$

where here j refers to the direction of motion. It is possible to determine a measure of the granular temperature by a direct calculation of the mean-squared velocities of the grains, but at high collision rates this is inaccurate as when the collision rate is comparable to the detection rate the instantaneous velocity is substantially underestimated. Current limitations with the PEPT facility mean that it is not yet possible to reliably measure granular temperature in this geometry, but we anticipate that improvements to both the PEPT facility and to the experimental rig will lead to this being achievable in the near future. We do, however, define granular temperature here, as it is a necessary component of the theoretical model that will be presented in §4.

2.2.3. *Mean velocity field*

The mean velocity was calculated through a centred finite-difference calculation performed for every coordinate location of the tracer particle. Typically the mean velocity was determined over ~ 20 ms of data for each calculation, and averaged over many measurements, the exact number depending on the length of the experiment and the size of the volume elements chosen for the analysis. Again, each of the components of the velocity field could be determined, resulting in a three-dimensional map of the full velocity field, $\boldsymbol{v}$. As with the other field quantities, the axial symmetry of the system allows the reduction of the dimensionality of the problem, with corresponding benefits to the signal-to-noise ratio of the measurements. In what follows, we use $v_{\theta r} = v_{\theta r}(\theta, r)$ to denote the θ and r components of $\boldsymbol{v}$ after integration along the z-direction. Likewise, $v_{rz} = v_{rz}(r, z)$ denotes the r and z components of the θ-integrated $\boldsymbol{v}$ distribution, and $v_\theta = v_\theta(z)$ is the θ component of $\boldsymbol{v}$ after integration over both θ- and r-directions.

3. Experimental results

3.1. *Packing Fraction*

Taking advantage of the axial symmetry of the annular shear cell, the packing fraction can be integrated over θ and projected onto a two-dimensional (r, z)-plane. Figure 4 shows the packing fraction distribution in the cell for the parameters: base angular velocity, $\omega = 9.74$ rad s^{-1} and confining pressure, $P^* = 0.0031$ where the pressure P has been non-dimensionalized by $\rho_s U^2$ and $\rho_s = 2.75 \times 10^3$ kg m^{-3} is the material density of the ballotini spheres, and where U is the speed of the lower boundary at the midpoint between the inner and outer walls; r^* and z^* are non-dimensional distances corresponding to r/σ and z/σ, respectively. Generally we observe that the packing fraction rises as we move up from the base, then peaks and at higher altitudes, and finally decays with height.

3.2. *Granular temperature*

The system geometry and the nature of the flow make measurements of the particle position rather difficult compared to, say, the motion of grains in a vibrated granular bed and we find that in our current set-up that the PEPT facility is only able to determine the position of the tracer particle at intervals of about 5 ms. The situation is further complicated when one considers the frequency at which a particle collides with the boundaries. Typically one sees the gap between the lower and the upper boundaries
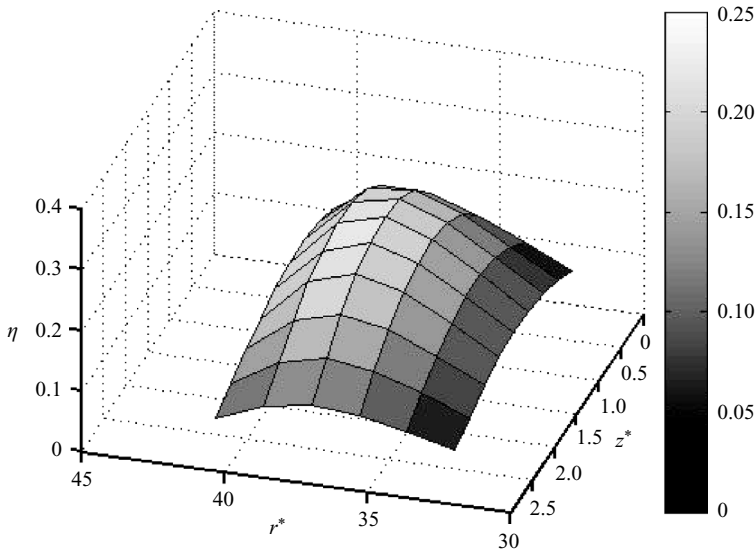
FIGURE 4. Packing fraction as a function of height and distance from the axis, non-dimensionalized using the particle diameter, σ, such that $z^* = z/\sigma$ and $r^* = r/\sigma$. The non-dimensional pressure exerted by the top boundary is $P^*(h) = 0.0031$ and the angular velocity of the base is $\omega = 9.74 \,\mathrm{rad\,s^{-1}}$.

to be about 2–3 particle diameters, and in the radial direction the separation is $\sim 8.3\sigma$. We can obtain a crude estimate of the frequency with which the particles collide with the wall by assuming an average of $h/4$ for the distance to the nearest boundary (where h is the vertical gap) and a mean speed of $\sim 0.3 \,\mathrm{m\,s^{-1}}$. This suggests that the mean time to a collision with the wall is $\sim 5\,\mathrm{ms}$, approximately equal to the time between detections in these experiments. With this relatively high particle–wall collision rate (compared to the detection rate), it is clear that under these conditions, direct calculation of the particle velocities or analysis of the mean-squared displacement (Wildman & Huntley 2000) will not give reliable data on the velocity fluctuations and we therefore limit ourselves to a study of the packing fraction and mean velocity field. However, forthcoming improvements to the PEPT facility and experimental setup suggest that a significantly improved spatial and temporal resolution is possible and we leave analysis of the granular temperature to future work.

3.3. *Mean velocity field*

Figure 5(a) shows a typical $v_{\theta r}$ velocity distribution for the case $\omega = 9.74 \,\mathrm{rad\,s^{-1}}$ and $P^* = 0.0031$. Quite clearly we see that, on average, the particle moves in the direction of the base (moving anticlockwise), with small velocity fluctuations about the mean. If we consider the motion in the (r, z)-plane we see that v_{rz} is small compared to $v_{\theta r}$, but it is not zero (figure 5b). The direction of the particles in this orientation is upwards at the outer wall and down at the centre. In three dimensions a particle being driven by the shear cell will, on average, take a helical path as it moves around the channel. In a linear shear cell one would not to expect to observe such features, and it occurs here due to the annular nature of the cell. In fact this type of secondary flow was first observed by Savage & Sayed (1984) in their preliminary experiments. In figure 5c we see that the angular velocity of the particles, v_θ (where the angular velocity of the
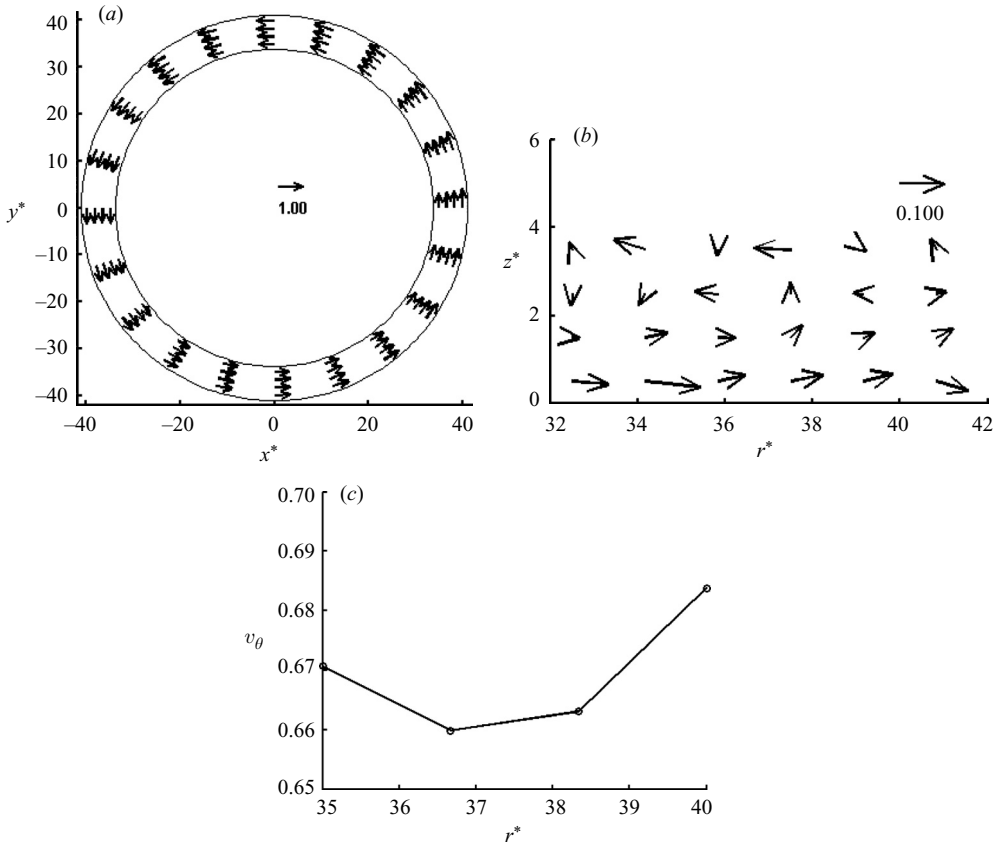
FIGURE 5. (a) Velocity field in the (θ, r)-plane, $\boldsymbol{v}^*_{\theta r}$, showing the average motion of the particles about the axis. The velocity and distances are non-dimensionalized such that $\boldsymbol{v}^*_{\theta r} = \boldsymbol{v}_{\theta r}/U$, $r^* = r/\sigma$ and $z^* = z/\sigma$. (b) Velocity field in the (r, z)-plane, v_{rz}, showing evidence for a secondary flow where particles flow up at the wall and down at the centre. Units are non-dimensionalized such that $v^*_{rz} = v_{rz}/U$, $z^* = z/\sigma$ and $r^* = r/\sigma$. (c) Magnitude of the non-dimensional angular velocity of the particles, v_θ, as a function of the distance from the axis, where $\alpha^* = \alpha/\omega$.

particles, v_θ, has been non-dimensionalized by angular velocity of the base, ω), across the cell width is not constant; the angular velocities are slightly larger nearer to the walls than in the bulk, suggesting, as a consequence of the sidewalls being attached to the lower driving boundary, that the particles are being dragged in the direction of base motion by the frictional interactions with the vertical boundaries.

3.4. *Experimental results discussion*

We observe variations in the packing fraction for (a) three values of the base speed ω of 6.50, 8.12 and 9.74 rad s^{-1} while keeping the pressure at the top surface P^* constant at 0.0031; and (b) four values of P^* of 0.0042, 0.0031, 0.0020 and 0.0009 while keeping ω fixed at 8.12 rad s^{-1}. Figure 6(a) shows the variation of η with the speed of the base. As the speed of the bottom boundary is increased, there is a dilation of the system and the thickness of the bed, h, increases. The dilation is determined by measuring distance between the upper and lower boundaries, with an error of the order of 1/3–2/3 particle diameters. This dilation is accompanied by a reduction in the average packing fraction as the particles become distributed over a greater volume. Figure 6(b)
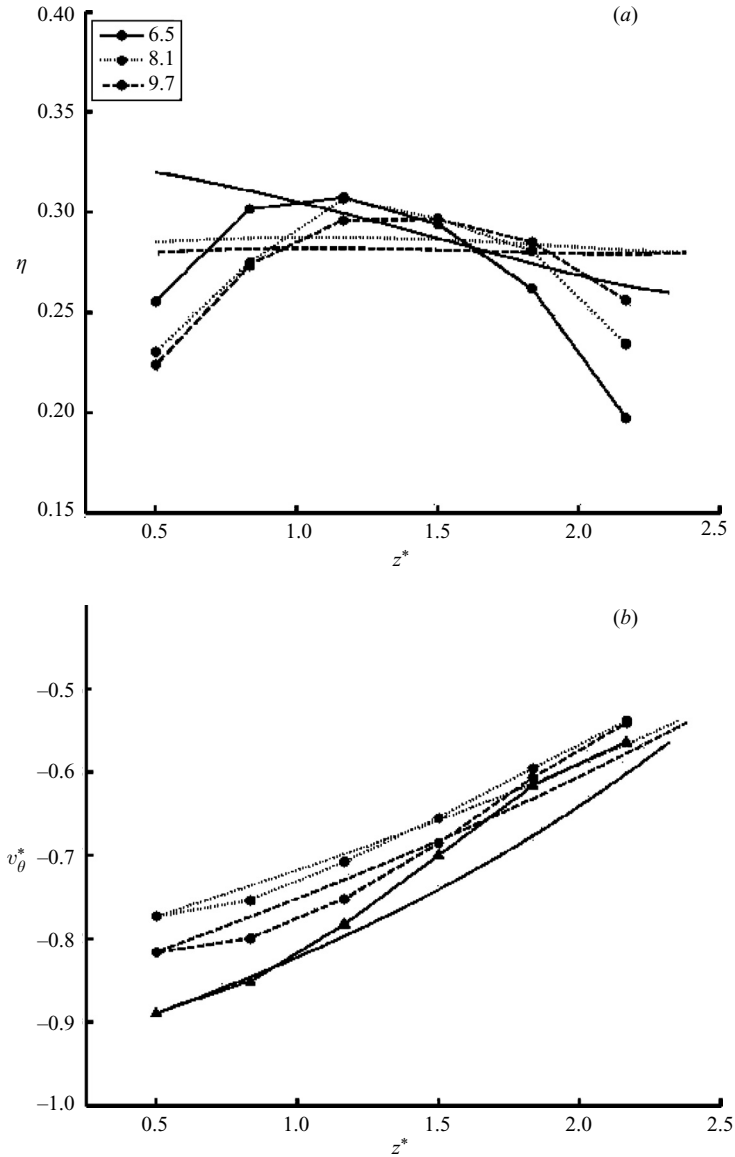
FIGURE 6. Comparison of the experimental results and the model predictions for (*a*) the packing fraction, η, and (*b*) the non-dimensional azimuthal velocity, $v_\theta^* = v_\theta / Us$ with non-dimensional height, $z^* = z/\sigma$, $P^* = 0.0031$. The legend shows the angular velocity of the base in units of rad s^{-1}. Experimental results are shown with symbols, whilst the theoretical predictions are shown with plain lines only.

shows the behaviour of the azimuthal velocity, v_θ^* of the particles as a function of the base angular velocity, ω, with a non-dimensional pressure exerted by the top boundary, $P^*(h) = 0.0031$. In our orientation, a non-dimensional speed $(v_\theta^* = v_\theta / U)$ of $v_\theta^* = -1$ is equivalent to the particles moving in an anticlockwise direction with speed U. In this, and in our subsequent one-dimensional model, we take U to be the velocity of the base at the mean distance of the channel from the axis of the shear cell

(112.5 mm). Near to the bottom boundary, we observe that the particles are moving fastest, whereas near to the top, close to the stationary boundary, they move slower, as one naturally expects. One also observes that there are significant slip velocities between the grains near the boundaries and the boundaries, of the order of 0.05–0.1 U at the base, and 0.4–0.5 U at the top. The curves also show a characteristic curved shape, with the gradient of the velocity (or shear rate) at a maximum towards the centre of the flow. The plateau near the edges is reminiscent of the packing fraction profile near to the base of a vibrated bed but is also possibly due to the finite spatial resolution of the PEPT facility, which leads to some of the particles being detected outside the cell. The convolution of the point spread function and the actual velocity profile would lead to a smooth plateau in the mean velocity near (inside and outside) the wall region. Finally, one observes that at this pressure, the scaled velocity fields are similar regardless of the magnitude of ω.

When the angular velocity at the base is kept constant and the pressure at the top boundary is varied, we see significant changes in the behaviour of the bed. Figure 7(a) shows the variation of the packing fraction with non-dimensional height, z^*. In general, as we increase the pressure, the bed contracts and the packing fraction near to the base increases. However, when the pressure on the bed is very low, the packing fraction qualitatively resembles that seen in, for example, a vibro-fluidized bed, where there is no confining top surface. Significant variations with pressure are also apparent in the velocity field $v_\theta(z)$ (figure 7b). As the pressure is increased, the velocity profiles are seen to move systematically upwards whilst maintaining a similar form. Also, as the pressure is increased, as we saw in figure 7(a), the particles sink towards the base, the slip velocity at the base reduces to almost zero, whilst the slip velocity at the top increases.

4. A kinetic-theory-based model for an annular shear cell

Experimental results at the single particle level can be used to test the predictions of kinetic-theory-based models. These models are necessary to understand the granular flow at the fundamental level, and serve as a vital component of models of systems ranging from the idealized experiments described in this paper, to descriptions of large-scale multiphase flows used in industrial operations.

In the regime where the particle interactions are dominated by instantaneous binary collisions, one can develop a hydrodynamic model based on the kinetic theory method. As discussed in the introduction to this paper, a number of researchers have developed constitutive relations to provide closure for the conservation equations for mass, momentum and energy. In this section we will follow the dense granular flow derivations of Jenkins and Richman for dry granular media, which provide constitutive relations for dense, but collisional flows of nearly elastic particles (Jenkins & Richman 1985b, 1986; Jenkins & Askari 1999).

4.1. *Conservation equations*

The differential forms for the equations of mass, momentum and energy have been derived specifically for granular flows (Jenkins & Askari 1999), but the general forms of these expressions are similar to those derived for thermal fluids. Three-dimensional expressions can be found in the literature (Slattery 1972; Arnarson & Jenkins 2004). Our system is a fully developed steady state with low velocity divergence and in our case the axial symmetry implies that the temperature gradient and hence heat
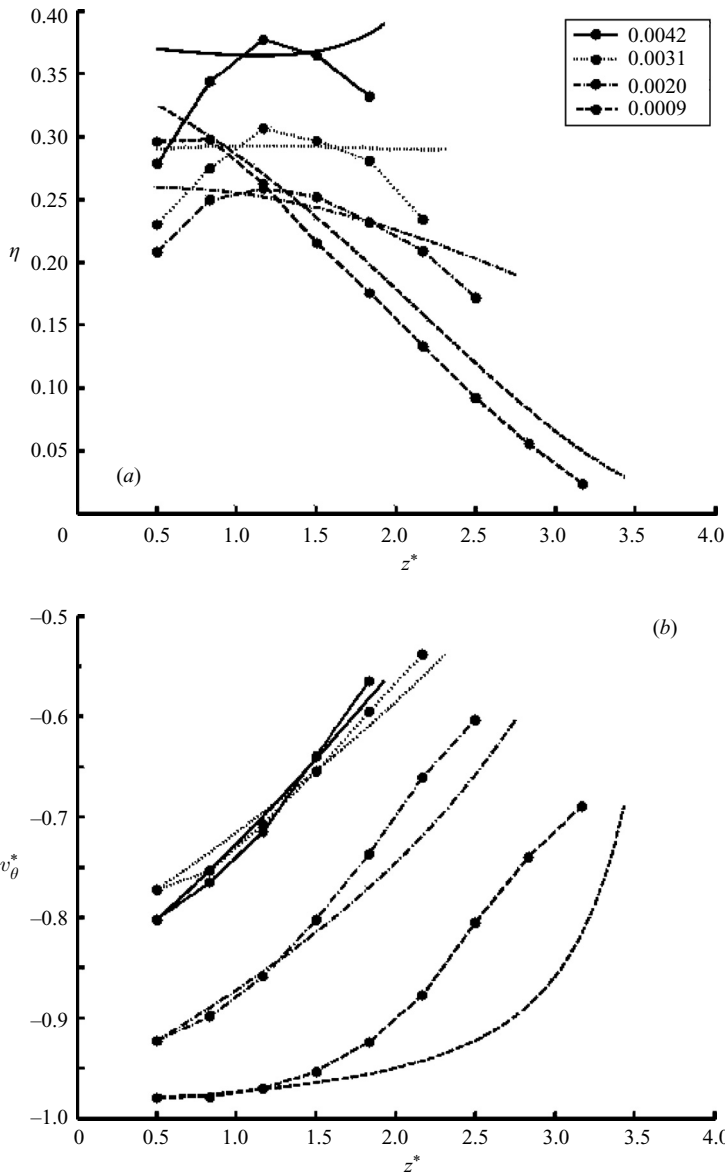
FIGURE 7. Comparison of the experimental results and the model predictions for (*a*) the packing fraction, η, and (*b*) the non-dimensional azimuthal velocity, $v_\theta^* = v_\theta/U$ with non-dimensional height $z^* = z/\sigma$, for $\omega = 8.12\,\text{rad s}^{-1}$. The legend shows the non-dimensional pressure exerted by the top boundary. Experimental results are shown with symbols, whilst the theoretical predictions are shown with plain lines only.

flux in the θ-direction is zero. We also make an approximation similar to that used in the analysis of vibro-fluidized beds (Martin *et al.* 2005) in assuming that the gradients in the r-direction are small. Evidence from vibro-fluidized beds suggests that even with high inelasticity at the walls gradients in r are much smaller than those in z (Viswanathan *et al.* 2006) and inspection of the experimental data supports this.

4.1.1. Filling

We fix the number of particles in the system through the use of an integral equation,

$$N\frac{\pi\sigma^3}{6A} = \int_0^h \eta \, \mathrm{d}z \tag{4}$$

where A is the area of the bottom boundary of the shear cell and h is the bed height. This equation is subsequently converted to an auxiliary ordinary differential equation which will be described in detail below (Arnarson & Jenkins 2004).

4.1.2. Momentum

One can consider an element that consists of a single horizontal slice of height $\mathrm{d}z$ and area A. The momentum transfer into and out of this slice reduces to a one-dimensional problem, and we only need to consider the vertical components, whilst we are able to neglect the bulk viscosity since the velocity divergence in a shear flow such as ours is negligible. The subsequent balance of forces in the z-direction leads to

$$\frac{\mathrm{d}P}{\mathrm{d}z} = -\frac{\mathrm{d}S}{\mathrm{d}z} - \rho g, \tag{5}$$

where

$$S = \frac{\sqrt{\pi}}{6} n\sigma T^{1/2} \left[\frac{5}{16}\frac{1}{G} + 1 + \frac{4}{5}\left(1 + \frac{12}{\pi}\right)G \right] \frac{\mathrm{d}v_\theta}{\mathrm{d}z} \tag{6}$$

where S is the shear stress, n is number density, and G (the product of the packing fraction and the radial distribution at contact, $g(\sigma)$) is given by

$$G = \frac{\eta(2-\eta)}{2(1-\eta)^3}, \tag{7}$$

and where P is the pressure. We use in (7) the form for $g(\sigma)$ suggested by Carnahan & Starling (1969).

4.1.3. Energy

In a granular system, the granular energy is not conserved owing to the loss of kinetic energy during collisions. The result of this is that in order to produce a hydrodynamic description of the energy transfer one must balance the transfer of energy into an element with the dissipation due to inelastic collisions. The one-dimensional energy balance on a slice is represented by

$$\frac{\mathrm{d}q_z}{\mathrm{d}z} - S\frac{\mathrm{d}v_\theta}{\mathrm{d}z} + \gamma = 0 \tag{8}$$

where the energy dissipation rate per unit volume, γ, is given by (Jenkins & Askari 1999)

$$\gamma = \frac{24}{\sqrt{\pi}}(1-e)\frac{PG}{(1+4G)}\frac{T^{1/2}}{\sigma}, \tag{9}$$

for which the heat flux law can be expressed as

$$q_z = -\kappa\frac{\mathrm{d}T}{\mathrm{d}z}. \tag{10}$$

The thermal conductivity, κ, is given by

$$\kappa = \frac{4MGP\sigma}{\sqrt{\pi}(1+4G)T^{1/2}} \tag{11}$$

and M is given by

$$M = 1 + \frac{9\pi}{32}\left(1 + \frac{5}{12G}\right)^2. \tag{12}$$

In this radially and azimuthally averaged one-dimensional problem, particle–wall dissipation cannot be included as a boundary condition but must instead be included in the bulk dissipation. The energy dissipation rate due to collisions (equation (9)) is then modified as follows:

$$\gamma = \frac{24(1-e)PGT^{1/2}}{\sqrt{\pi}\sigma(1+4G)m^{1/2}} + \frac{2}{\overline{R}}\left(\frac{2}{\pi}\right)^{1/2} P\left[(1-e_w)(T/m)^{1/2}\right] \tag{13}$$

where $\overline{R}$ is the distance from the axis to the midpoint between the inner and outer boundaries (Richman 1993; Martin *et al.* 2005).

In this form the conservation equations simplify considerably into a set of first-order ordinary differential equations that can be solved numerically using the Matlab bvp4c boundary problem solver (Kiezenka & Shampine 2001). The problem is then solved by combining the conservation equations with the transport equations (6), (11) and (13) and the equation of state,

$$P = \eta T(1+4G), \tag{14}$$

together with the boundary conditions (§ 4.2).

4.2. *Boundary conditions*

A number of researchers have proposed relations that describe the transfer of energy and momentum at a boundary, e.g. Richman (1993). These equations consider the collision details between particles and the wall and use a kinetic theory approach to describe the heat and momentum fluxes. It is possible to use these relations for our shear flow system, but they are strictly applicable to 'bumpy' boundaries rather than sawtooth profiles and our preliminary studies suggested that, for our system, the relations of Richman would not result in a good match. For this reason, we allow the experimental results to serve as boundary conditions or constraints on the model and compare the bulk profiles rather than specifying relations for the heat and momentum flux at the boundaries.

The number of ODEs in the system in combination with the need for a constant-pressure condition means that we must employ six constraints to close the equation set. First, we express the filling condition in the form of an ODE with two boundary conditions. Our first step is to restate (4) using the auxiliary equation

$$I(z) = \int_0^z \eta(\xi)\,\mathrm{d}\xi \tag{15}$$

such that

$$\frac{\mathrm{d}I(z)}{\mathrm{d}z} = \eta(z), \tag{16}$$

which serves as an extra ODE. This has two boundary conditions:

$$I(0) = 0 \tag{17}$$

and

$$I(h) = N\frac{\pi\sigma^3}{6A}. \tag{18}$$

To allow the top surface to find its steady state height, we provide a further condition, namely that the pressure at the top must be equal to the pressure due to

the weight of the top surface, P_h, i.e.

$$P(h) = P_h \qquad (19)$$

where h now serves as an extra variable and allows us to solve for the bed thickness.

The other conditions are specified by using measured values of the packing fraction and the velocity field. The velocity field at the upper and lower boundary are used as inputs to the solver. The measurements of the packing fraction, however, are least reliable near to the wall and so we estimate the values at the wall and iterate around these values until the model agrees with experimentally determined packing fractions at ∼1 particle diameter from the boundaries.

5. Model predictions and comparison with experimental results

Figures 6(a) and 6(b) show a comparison of the predicted packing fraction and velocity fields for P fixed and ω varying using the same parameters for the model as used in experiment and employing the constraints described in §4. We do not show the full range of data since the dependence on ω is very weak. Varying ω causes only relatively small changes in the packing fraction and it is difficult to determine trends. There are some discrepancies between model and experiment close to the boundaries, which can be attributed to the point spread function associated with the PEPT facility (Wildman *et al.* 2001*b*) and demonstrate the need to match the packing fractions in the centre of the flow. The form of the profiles for the mean velocity, v_θ, is similar for both experiment and theory. One possible improvement to the comparison could be to use more accurate, but significantly more complex theories (e.g. those of Brey *et al.* 1998; Sela & Goldhirsch 1998; Garzo & Dufty 1999). The difference in the results produced by these theories is, however, typically of the order of a few percent, and these are not sufficient to explain the differences observed (Galvin, Hrenya & Wildman 2007). Away from the boundary region, the packing fraction decreases with height, and as the speed of the base is increased we see more dilation and a reduction in the average packing fraction. The free parameter h is in good agreement with the experimental results.

Figures 7(a) and 7(b) show the behaviour of the system when we vary P and keep ω constant (table 2). As we vary the pressure we find that the forms of the packing fraction prediction appear much as for the experiments, though there are differences near to the boundaries. As the pressure on the system is reduced the cell dilates and the packing fraction decreases. Usually, the packing fraction at the upper boundary is lower than at the bottom boundary and this effect becomes more marked as the pressure is reduced. At the lowest pressure value studied ($P^* = 0.0009$), the profile is reminiscent of that seen in a vibrated granular bed (Wildman *et al.* 2001*b*; Martin *et al.* 2005) for which, we recall, the confining pressure is zero.

Turning to the velocity field (figure 7b), the data show that the form of the velocity profile changes significantly as we reduce the confining pressure: the slip velocity at the base decreases and the particles are more likely to flow along with the base. This is compensated for by an increase in the slip velocity at the top boundary. The net result is that the reduction in pressure leads to an increase in the flow rate of the particles around the cell. However, the velocity gradient stays broadly the same, suggesting that the shear work done in each case is similar. At the very lowest pressure, however, the velocity gradient starts to vary strongly with position across the depth and a significant increase in shear is observed near to the top boundary. At the higher pressures, v_θ varies almost linearly with height and this, combined with

the minor variations in the packing fraction, is reminiscent of a flow observing the Bagnold flow rule (Mitarai & Nakanishi 2005).

6. Discussion

This first step in measurement of the behaviour of a granular bed undergoing rapid shear flow using PEPT has demonstrated the potential of the technique for probing complex granular flow. We have been able to make detailed measurements of the concentration and mean velocity profiles and compare them to a model based on kinetic theory. (Jenkins & Richman 1985b; Jenkins & Askari 1999). The capture of the general forms of the observed behaviour by the model suggests that the basic physics is described, although the weak dependence on ω leads to some difficulties in discrimination. In this study, we do not include independent boundary conditions, owing to the difficulties in describing this part of the flow well due to the sawtooth profile and the presence of a Knudsen-like layer that extends from the boundary and into the system. In the future details such as this should be incorporated into descriptions of granular flows and need to be addressed. We have also ignored the centripetal accelerations in the analysis and neglected any modifications due to the radial variations in packing fraction and granular temperature that result from the geometry of the system. It is clear, however, from the presence of the secondary flows, that these variations have consequences that are difficult to predict using a one-dimensional model and suggest a two-dimensional solution of the conservation equations is required to fully describe the system. Future studies will focus on improving the ability of the PEPT facility to measure the granular temperature, addressing the boundary heat and momentum transfer and developing a two-dimensional model for predicting all three components of the velocity field.

7. Conclusions

For the first time some of the key variables within a three-dimensional dry granular medium undergoing rapid shear have been measured. Using positron emission particle tracking, we were able to determine the packing fraction and mean velocity as a function of position within the annular shear cell. This work has highlighted the power of positron emission particle tracking for determining the behaviour of three-dimensional granular flows and we were able to show, at least for the quantities that could be measured experimentally, that the model predicts the qualitative behaviour of the shear flow reasonably well.

REFERENCES

Arnarson, B. O. & Jenkins, J. T. 2004 Binary mixtures of inelastic spheres: Simplified constitutive theory. *Phys. Fluids* **16**, 4543–4550.

BIZON, C., SHATTUCK, M. D., SWIFT, J. B., MCCORMICK, W. D. & SWINNEY, H. L. 1998 Patterns in 3d vertically oscillated granular layers: Simulation and experiment. *Phys. Rev. Lett.* **80**, 57–60.

BREY, J. J., DUFTY, J. W., KIM, C. S. & SANTOS, A. 1998 Hydrodynamics for granular flow at low density. *Phys. Rev.* E **58**, 4638–4653.

BREY, J. J., RUIZ-MONTERO, M. J. & MORENO, F. 2001 Hydrodynamics of an open vibrated granular system. *Phys. Rev.* E **63**, 061305.

CAMPBELL, C. S. 2002 Granular shear flows at the elastic limit. *J. Fluid Mech.* **465**, 261–291.

CARNAHAN, N. F. & STARLING, K. E. 1969 Equation of state for nonattracting rigid spheres. *J. Chem. Phys.* **51**, 635–636.

CHAPMAN, S. & COWLING, T. G. 1970 *The Mathematical Theory of Non-uniform Gases*. Cambridge University Press.

CLEMENT, E. & RAJCHENBACH, J. 1991 Fluidization of a bidimensional powder. *Europhys. Lett.* **16**, 133–138.

GALVIN, J. E., HRENYA, C. M., & WILDMAN, R. D. 2007 On the role of the Knudsen layer in rapid granular flows. *J. Fluid Mech.* **585**, 73–92.

GARZO, V. & DUFTY, J. W. 1999 Dense fluid transport for inelastic hard spheres. *Phys. Rev.* E **59**, 5895–5911.

HELAL, K., BIBEN, T. & HANSEN, J. P. 1997 Local fluctuations in a fluidized granular medium. *Physica* A **240**, 361–373.

HSIAU, S. S. & SHIEH, Y. M. 1999 Fluctuations and self-diffusion of sheared granular material flows. *J. Rheol.* **43**, 1049–1066.

HUAN, C., YANG, X. Y., CANDELA, D., MAIR, R. W. & WALSWORTH, R. L. 2004 NMR experiments on a three-dimensional vibrofluidized granular medium. *Phys. Rev.* E **69**, 041302.

JENKINS, J. T. & ASKARI, E. 1999 Hydraulic theory for a debris flow supported on a collisional shear layer. *Chaos* **9**, 654–658.

JENKINS, J. T. & MANCINI, F. 1989 Kinetic-theory for binary-mixtures of smooth, nearly elastic spheres. *Phys. Fluids* A **1**, 2050–2057.

JENKINS, J. T. & RICHMAN, M. W. 1985a Grads 13-moment system for a dense gas of inelastic spheres. *Arch. Rat. Mech. Anal.* **87**, 355–377.

JENKINS, J. T. & RICHMAN, M. W. 1985b Kinetic-theory for plane flows of a dense gas of identical, rough, inelastic, circular disks. *Phys. Fluids* **28**, 3485–3494.

JENKINS, J. T. & RICHMAN, M. W. 1986 Boundary-conditions for plane flows of smooth, nearly elastic, circular disks. *J. Fluid Mech.* **171**, 53–69.

JENKINS, J. T. & SAVAGE, S. B. 1983 A theory for the rapid flow of identical, smooth, nearly elastic, spherical-particles. *J. Fluid Mech.* **130**, 187–202.

JOHNSON, P. C., NOTT, P. & JACKSON, R. 1990 Frictional collisional equations of motion for particulate flows and their application to chutes. *J. Fluid Mech.* **210**, 501–535.

KIERZENKA, J. & SHAMPINE, L. F. 2001 A bvp solver based on residual control and the MATLAB PSE. *ACM Trans. Math. Software.* **27**, 299–316.

KUMARAN, V. 1998a Kinetic theory for a vibro-fluidized bed. *J. Fluid Mech.* **364**, 163–185.

KUMARAN, V. 1998b Temperature of a granular material "fluidized" by external vibrations. *Phys. Rev.* E **57**, 5660–5664.

LOUGE, M. Y. 2003 Model for dense granular flows down bumpy inclines. *Phys. Rev.* E **67**, 061303.

LU, H. L., GIDASPOW, D. & MANGER, E. 2001 Kinetic theory of fluidized binary granular mixtures. *Phys. Rev.* E **6406**, 061301.

LUDING, S., HERRMANN, H. J. & BLUMEN, A. 1994 Simulations of 2-dimensional arrays of beads under external vibrations – scaling behavior. *Phys. Rev.* E **50**, 3100–3108.

MARTIN, T. W., HUNTLEY, J. M. & WILDMAN, R. D. 2005 Hydrodynamic model for a vibrofluidized granular bed. *J. Fluid Mech.* **535**, 325–345.

MCNAMARA, S. & LUDING S. 1998 Energy nonequipartition in systems of inelastic, rough spheres. *Phys. Rev.* E **58**, 2247–2250.

MIDI, G. D. R. 2004 On dense granular flows. *Eur. Phys. J.* E **14**, 341–365.

MITARAI, N. & NAKANISHI, H. 2005 Bagnold scaling, density plateau, and kinetic theory analysis of dense granular flow. *Phys. Rev. Lett.* **94**, 128001.

PARKER, D. J., ALLEN, D. A., BENTON, D. M., FOWLES, P., MCNEIL, P. A., TAN, M. & BEYNON, T. D. 1997 Developments in particle tracking using the birmingham positron camera. *Nucl. Instrum. Meth. Phys. Res.* **392**, 421–426.

RICHMAN, M. W. 1993 Boundary-conditions for granular flows at randomly fluctuating bumpy boundaries. *Mech. Mater.* **16**, 211–218.

SAVAGE, S. B. & SAYED, M. 1984 Stresses developed by dry cohesionless granular-materials sheared in an annular shear cell. *J. Fluid Mech.* **142**, 391–430.

SELA, N. & GOLDHIRSCH, I. 1998 Hydrodynamic equations for rapid flows of smooth inelastic spheres, to Burnett order. *J. Fluid Mech.* **361**, 41–74.

SLATTERY, J. C. 1972 *Momentum, Energy and Mass Transfer in Continua*. McGraw-Hill.

SUNTHAR, P. & KUMARAN, V. 1999 Temperature scaling in a dense vibrofluidized granular material. *Phys. Rev.* E **60**, 1951–1955.

TALBOT, J. & VIOT, P. 2002 Wall-enhanced convection in vibrofluidized granular systems. *Phys. Rev. Lett.* **89**, 064301.

TSUJI, Y., MORIKAWA, Y. & SHIOMI, H. 1984 LDV measurements of an air solid 2-phase flow in a vertical pipe. *J. Fluid Mech.* **139**, 417–434.

UMBANHOWAR, P. B., MELO, F. & SWINNEY, H. L. 1996 Localized excitations in a vertically vibrated granular layer. *Nature* **382**, 793–796.

VISWANATHAN, H., WILDMAN, R. D., HUNTLEY, J. M. & MARTIN, T. W. 2006 Comparison of kinetic theory predictions with experimental results for a vibrated three-dimensional granular bed. *Phys. Fluids* **18**, 113302.

VOLFSON, D., TSIMRING, L. S. & ARANSON, I. S. 2003 Order parameter description of stationary partially fluidized shear granular flows. *Phys. Rev. Lett.* **90**, 254301.

WARR, S., HUNTLEY, J. M. & JACQUES, G. T. H. 1995 Fluidization of a 2-dimensional granular system – experimental study and scaling behavior. *Phys. Rev.* E **52**, 5583–5595.

WILDMAN, R. D. & HUNTLEY, J. M. 2000 Novel method for measurement of granular temperature distributions in two-dimensional vibro-fluidised beds. *Powder Technol.* **113**, 14–22.

WILDMAN, R. D., HUNTLEY, J. M., HANSEN, J. P., PARKER, D. J. & ALLEN, D. A. 2000 Single-particle motion in three-dimensional vibrofluidized granular beds. *Phys. Rev.* E **62**, 3826–3835.

WILDMAN, R. D., HUNTLEY, J. M. & PARKER, D. J. 2001a Convection in highly fluidized three-dimensional granular beds. *Phys. Rev. Lett.* **86**, 3304–3307.

WILDMAN, R. D., HUNTLEY, J. M. & PARKER, D. J. 2001b Granular temperature profiles in three-dimensional vibrofluidized granular beds. *Phys. Rev.* E **6306**, 061311.

WILDMAN, R. D. & PARKER, D. J. 2002 Coexistence of two granular temperatures in binary vibrofluidized beds. *Phys. Rev. Lett.* **88**, 064301.

YANG, X. Y., HUAN, C., CANDELA, D., MAIR, R. W. & WALSWORTH, R. L. 2002 Measurements of grain motion in a dense, three-dimensional granular fluid. *Phys. Rev. Lett.* **88**, 044301.

ZAMANKHAN, P. 1995 Kinetic-theory of multicomponent dense mixtures of slightly inelastic spherical-particles. *Phys. Rev.* E **52**, 4877–4891.